Bio and electronically controlled surface plasmons polaritons generated by coupling between nano-antenna and photosynthetic protein - photosystem I

Itai Carmeli
Tel-Aviv University
Ibrahim Tanriover
Northwestern University
Tirupathi Malavath
Tel Aviv University
chanoch carmeli
tel aviv University
Moshik Cohen
Bar-Ilan University
Yossi Abulafia
Bar-Ilan Institute for Nanotechnology & Advanced Materials
Olga Girshevitz
Bar-Ilan University
Shachar Richter
Tel Aviv University
Koray Aydin
Northwestern University https://orcid.org/0000-0002-3268-2216
Zeev Zalevsky (zeev.zalevsky@biu.ac.il)
Bar Ilan University https://orcid.org/0000-0002-4459-3421

Article

Keywords:

Posted Date: November 11th, 2022

DOI: https://doi.org/10.21203/rs.3.rs-2163297/v1

Additional Declarations: There is **NO** Competing Interest.

Bio and electronically controlled surface plasmons polaritons generated by coupling between nano-antenna and photosynthetic protein - photosystem I

Itai Carmeli, Ibrahim Tanriover, Tirupathi Malavath, Chanoch Carmeli, Moshik Cohen, Abulafia Yossi, Olga Girshevitz, Shachar Richter, Koray Aydin, Zeev Zalevsky

Abstract

Surface plasmons polaritons (SPP) hold great promise for the next generation of fast nanoscale optoelectronic devices, as silicon-based electronic devices approach fundamental speed and scaling limitations. However, in order to fully exploit the potential of plasmonics, devices and material systems capable of actively controlling and manipulating plasmonic response is essential. Here, we demonstrate active control of the electric field distribution of a micro antenna by coupling SPP to a photosynthetic protein with outstanding optoelectronic properties and long range and efficient exciton transfer ability. The hybrid bio-solid state active platform is able to tune and modulate the optical activity of a micro plasmonic antenna via interaction of the bioactive material with plasmon oscillations occurring in the antennae. In addition, we demonstrate that the effect of the coupling can be further enhanced and controlled by an external potential applied to the micro antenna Photosynthetic hybrid system.

Introduction

Surface plasmon nanophotonics holds great promise for fast data processing due to the unprecedented capability of plasmons to enhance light-matter interactions and confine light into deep-subwavelength scale. Plasmon-enhanced nanophotonic devices are poised to overcome the limitations of current silicon-based electronic devices approaching fundamental speed and scaling limitations[1]. Plasmonic nanoantenna[2–5], waveguides[6–9] and devices[10–12] unlock an enormous potential for exciting new applications based on surface plasmons polaritons (SPPs). Surface plasmon polaritons (SPPs), often abbreviated to plasmons, are collective oscillations of the conduction electrons driven by light at the surfaces of metals[13–15]. As such, the plasmons oscillate at optical frequencies enabling strongly localized electric field distributions. As plasmons can be confined to regions 100 times smaller than light focused to a diffraction-limited spot, they provide an unprecedented means to manipulate optical energy at the nanoscale. However, in order to exploit these

properties, active manipulation of SPP interactions is required. By their very nature, SPP fields are strongly confined at metal surfaces and therefore highly sensitive to refractive index changes within a few tens of nanometres of the surface[16]. The basic idea in active plasmonic systems is to induce transient change in SPP through the interface with the dielectric coating. It was shown that by coupling of plasmons to electro-optic media, quantum dots, photochromatic molecules, graphene, or phase-change materials, modulation of the SPP signal can be achieved[16]. Active plasmonic devices have the ability to tune and dynamically control optical properties using electrical, optical, mechanical or thermal external stimulation.

In this work, we report the first successful attempt in integration of a photosynthetic protein - Photosystem I (PS I), to plasmonic antennae. This protein was chosen due to its extended antenna system which captures light efficiently and transfer its energy by a quantum coherence highly efficient exciton transfer mechanism, as been suggested in recent work[17]. Our hybrid bio-solid state active platform is able to tune and modulate the optical activity of a micro plasmonic antenna via interaction of the bioactive material with plasmon oscillations occurring in the antennae. We experimentally study and simulate the molecular effect on plasmon distribution and electric potential of a gold micro electrode coated with various thin films of photosystem complexes. Of particular interest is the response of the hybrid system to applied voltage in the purpose of having control over the electric field distribution of a plasmonic antenna by externally applied voltage. To achieve high spatial resolution of the SPP electric field distribution, we use Kelvin Force Microscopy (KPFM) an effective alternative method to near field spectroscopy, due to its high spatial measurement capabilities. This method allows visualizing localized plasmons and their electric field distribution on a single nanometer scale, as previously demonstrated by us[18].

Results

The hybrid system. In order to perform a detailed and diverse investigation, we utilized four different types of photosynthetic films antenna coatings embedding the photosynthetic protein Photosystem I (PS I):

1. Single PS I monolayer.

2. Multilayer containing four oriented layers of PS I.

3. Metal-PS I nano composites of gold colloids hybridized with PS I.

4. Metal-PS I nano composites of silver nano particles hybridized with PS I.

Photosynthetic proteins such as the photosystem I are nature's most efficient light harvesting complexes known to exhibit outstanding optoelectronic properties. PS I was chosen for this study due to its outstanding optoelectronic properties and its long range and efficient exciton and electron transfer[17,19–23]. PSI is a transmembrane multi-subunit protein-chlorophyll complex that mediates vectorial light-induced electron transfer.

The PS I used in this study, derived from cyanobacterial membrane, is a nano-size protein-chlorophyll complex, which integrates 96 chlorophyll and 22 carotenoid pigment molecules in a helical protein membrane complex. It harvests photons with a quantum efficiency of ~1, and was found to be stable and photoactive when adsorbed in a dry environment[20,24,25]. This efficient and robust system exhibits a quantum yield close to 100%, with an energy yield around 58%. The nano-size protein has the potential to serve as an active component in optoelectronic devices and have potential use in the growing field of hybrid bioelectronics applications in molecular optoelectronics, such as a protein based solar cell, a nano energy source to power nano electronic circuits, and an efficient sensor for light[26–28]. Recently, we demonstrated the feasibility of PS I as an active material in plasmonics to spatially modulate light transmission through a metallic microslit[26].

Hybrid Sample fabrication Self-assembled mono and multi-layers of PS I were fabricated by formation of a direct sulfide bond between unique cysteine mutants in PS I and the antenna gold surface on chip (Method section). The advantage of this technique compared to spin coating is that here the surface of the gold is coated with covalently bound material with only a thin (few tenths of nanometer) of organized and oriented organic thin film. Multilayers were fabricated by crosslinking of successive PS I layers. This technique ensures that the PS I multilayer is covalently bonded to the surface in an oriented in a vectorially fashion[26]. Gold and silver PS I nano colloids were prepared as previously described[29]. In short, silver or Au ions in buffer solution were reduced with sodium borohydride (NaBH4) in the presence of the PS I. The reduction caused the formation of hybrid metal-PS I nanoparticles in which the PS I protein is embedded within the metal framework. Hybrid nanoparticles were absorbed

onto the antenna in the same manner as of the isolated PS I. AFM images indicate dense coverage of nanoparticles on the surface with thicknesses ranging from 5 nm to 15 nm for various films (Fig.S1).

Voltage dependent surface potential measurements. The antenna system was designed such that it is connected at opposite ends to a micro electrode that enables application of voltage to the antenna (see Fig.1). Voltages in the range of 0V to 0.6V were applied to one end of the antenna, while the opposite end was grounded. The surface potentials (CPD) for the various coatings were recorded for different electrode voltages while illuminated with continuous white light source. Results are then compared with the uncoated reference antenna sample. Figure-1 shows the surface potential of an antenna coated with Ag-PS I hybrid colloids for three different gate voltage values. It is seen that the potential is concentrated mainly at the ends of the antenna and increases with increased voltage applied to the electrodes.

Ag-PSI hybrid antenna system

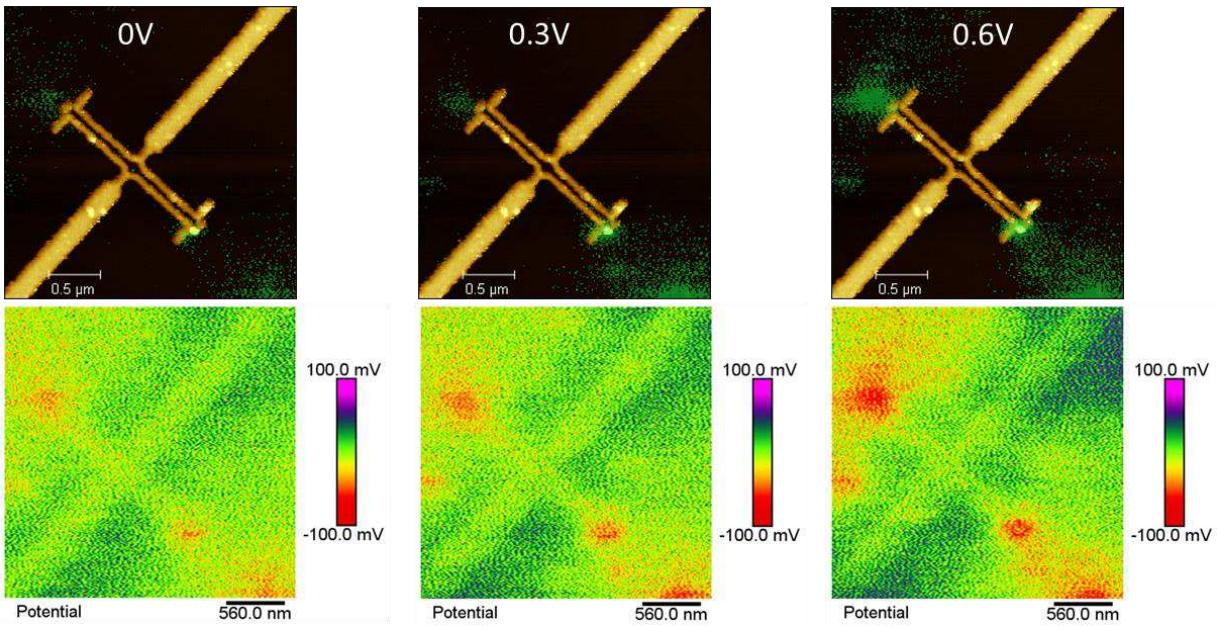

Figure 1: Surface potential (CPD) of Ag colloids-PS I hybrid antenna system at various external voltages applied to the electrodes connected to opposite sides of the antenna. Top row: Overlay of the surface potential on topography images of the antenna system. Bottom row: Plain surface potential images of the hybrid antenna system.

Next is the case for an antenna coated with Au-PS I hybrid colloids (Fig.2). Here, a similar behavior to the Ag-PS I hybrid colloids is observed where the electric field is

concentrated mostly at the ends of the antenna. The difference is that for the Au coating case, the electric field distribution is more diffused.

Au-PSI hybrid antenna system

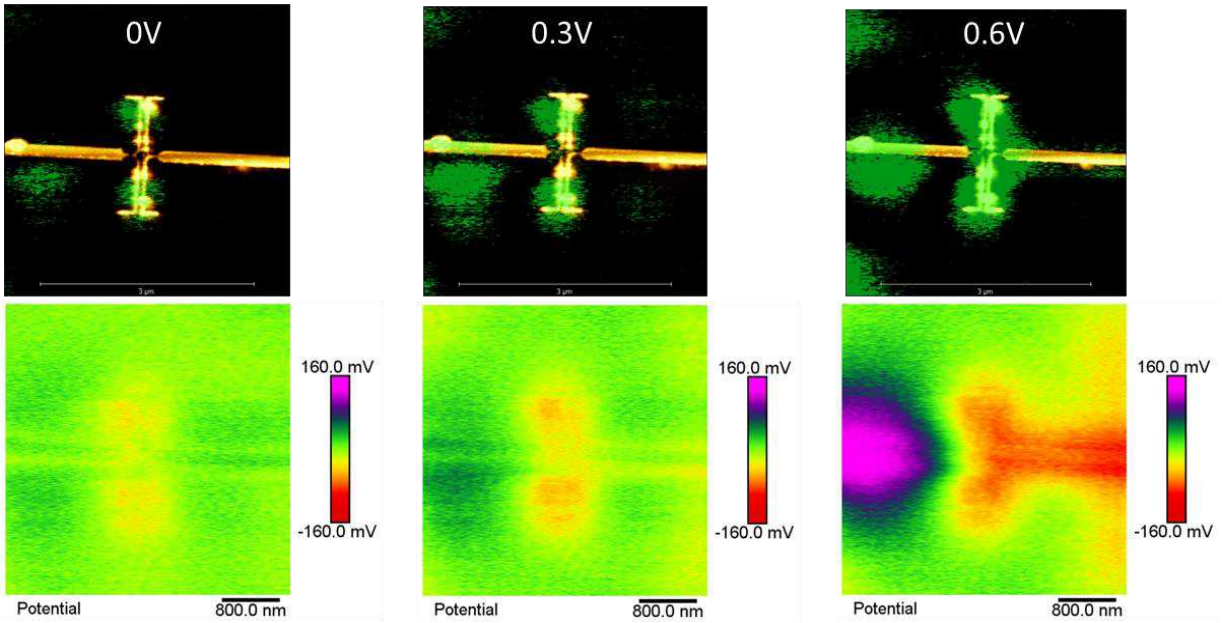

Figure 2: Surface potential (CPD) of Au colloids-PSI hybrid antenna system at various external voltages applied to the electrodes connected to the antenna. Top row: Overlay of the surface potential on topography images of the antenna system. Bottom row: Plain surface potential images of the hybrid antenna system.

In the case where the antenna coating is a single PS I layer, the observed effect is different (see Fig. S2a). In this case the electric field concentrates at the center and not at the ends as in the metal colloid-PS I hybrid case, and increases with increasing gate potential.

For a 4 PS I multilayer coating the situation is similar to that of the single layer coating (Fig. S2b) however the formation of multilayer increases the electric field on the antenna and the electrodes as well. The surface roughness created by adsorption of four PS I layers can clearly be seen in the AFM images (Fig.S1b).

Last, is a comparison to an uncoated reference antenna. We observe that the reference antenna acts as a capacitor with increasing electric field intensity as function of the applied external voltage.

Uncoated reference antenna

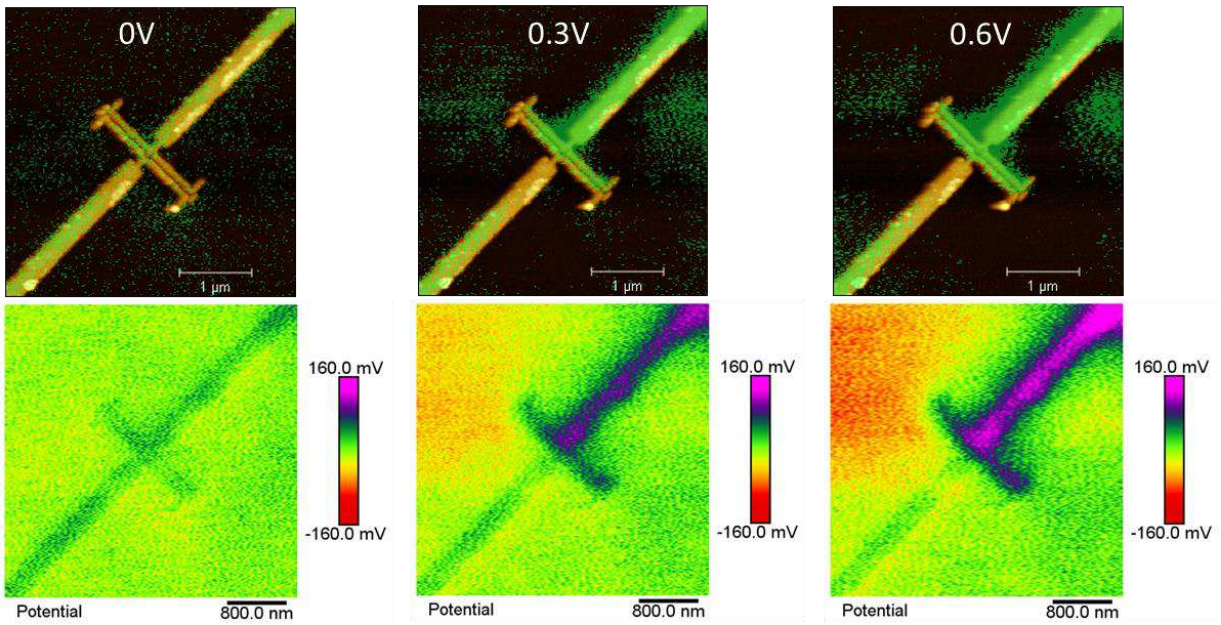

Figure 3: Surface potential (CPD) of the uncoated reference antenna at various external voltages applied to the electrodes connected to the antenna. Top row: Overlay of the surface potential on topography images of the antenna system. Bottom row: Plain surface potential images of the hybrid antenna system.

The difference in the electric field between the coated and uncoated antenna systems is summarized in a graph Fig.S3 (supplementary section). Comparison of the coated to the uncoated antenna shows that while the uncoated antenna resembles a capacitor with an even potential distribution across the antenna, the molecular coating concentrates the potential as dipoles on the antenna depending on the coating preference. Another evident difference between the coated and uncoated antennas is that the coating reverses the sign of the CPD compared with the uncoated antenna. This can be attributed to charge transfer between the metal interface and the coating as been previously observed[20,24,25]. When looking at the difference between the films we see that the Ag-PS I and Au-PS I colloids created a dipole, that is, the electric field radiates mostly at the ends of the antenna. From the potential cross-sections (Fig.S3, top row) and the potential images (Fig.1-2) it is evident that for both coatings the potential is concentrated at the ends of the antenna as indicate by the red and green arrows for the Ag and Au PS I coatings, respectively. This is in contrast to the molecular coating containing no metal colloids where the electric field is mostly concentrated at the center of the antenna (Fig.S3, bottom row) as indicated by the blue

and gray arrows for the single and multilayer coatings, respectively. For all coatings, the external applied voltage at the electrodes increases the electric field of the antenna where it is concentrated. The enhancement is more pronounced however in the molecular system (no colloids) at higher externally applied voltages.

Simulations

We simulated the electric field distributions over the coated and uncoated antenna systems under white light illumination without voltage bias using commercial simulation software Ansys Lumerical FDTD. We placed the antenna on top of a Si substrate and located it at the middle of the simulation region (over *xy* plane) and a broadband plane wave source is placed above the structures (+z side) with the injection axis parallel to the surface normal (-$\hat{z}$). The connectors were also included in the simulation model as finite size Au bars. The antenna-connector structure was covered with PS I and the Ag and Au nanoparticles were randomly distributed over the structure surface when applicable. Unpolarized illumination is applied and field distributions were recorded at fundamental planes (See methods for simulation details). Overall, the simulations reveal good correlation with the experimental results.

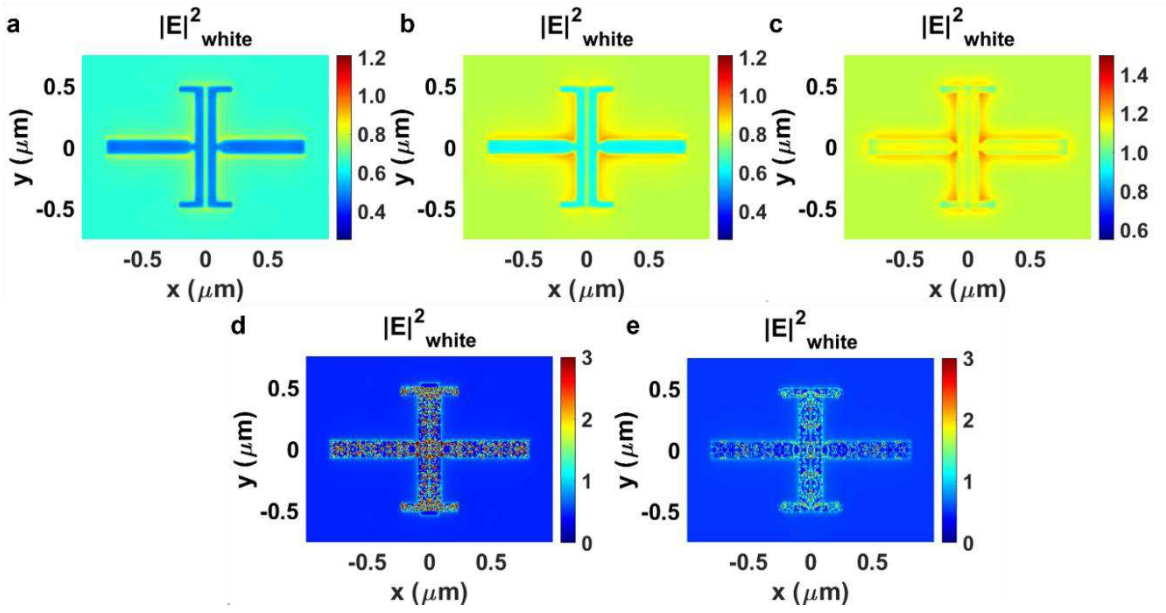

Figure 4: Distribution of simulated electric field squared over (a) uncoated antenna (b) PS I single layer (c) PS I multilayer (d)Ag-PSI film (e) Au-PSI film. Illumination by unpolarized white light with perpendicular incidence is considered in simulations.

As seen in the Fig. 4a-c, the field is mostly scattered by the antenna. However, from uncoated antenna (Fig. 3) to multilayer PS I coated antenna (Fig. S2b), field localization over antenna evidently increases with increased PS I content due to absorption from PS I (Fig. S4). As seen in the Fig. 4b,c, the localized field distributed over both the antenna and connectors and it is stronger in multilayer PS I case than that of single layer PS I in accordance with the experimental results Fig. S2. The field scattering from antenna is not observed in case of metal-PS I hybrid colloids since Au and Ag nanoparticles create strong field confinement on their surface, which dominates over other effects as seen in Fig. 4d,e and Supplementary Figure 4. We observe in the simulation especially noticeable in the Au-PS I situation (Fig. 4e), standing waves with round electric field distribution nearing the edge of the antenna, in good correlation with experiment (Fig. 2). The intensity of these concentrated electric fields are about 2-3time stronger than of the uncoated antenna in the Au-PSI case and ~4 times stronger in the Ag-PS I coating at these specific locations (See Fig. S3 top row, indicated by the green and red arrows). This is in correlation with the experimental results and interestingly, also in agreement with previous predictions and studies[29] that showed enhancement of light absorption of PS I coupled to Au and Ag colloids by a factor of ~2.5 and 4, Respectively. Overall, the simulated field distributions (Fig. 4) are in parallel with the Voltage measurements (Fig. 1-2 and Fig. S2a,b). Consequently, we attribute the results observed from surface potential measurements to field induced exciton generation. The localized field is absorbed by the PS I, which creates excitons. Applied DC bias spatially separates the electrons and holes, which breaks the binding within excitons and converts them to free charge carriers. This, in turn, induces conductivity as seen in Eqn. 1;

$$\frac{1}{\rho} = \sigma = q n_{ex}(\mu_e + \mu_h) \qquad (1)$$

where ρ is resistivity, σ is conductivity, q is electron charge, n_{ex} is free charge carrier (electron-hole) concentration, and $\mu_{e(h)}$ is electron (hole) mobility. To calculate the potential distribution, the antenna can be discretized into smaller regional portions each having the resistance of

$$R = \rho \frac{l}{A} \qquad (2)$$

where R is the resistance, ρ is resistivity, l is the length, and A is the cross-sectional area of the region of interest. The electric potential of a region is calculated as

$$V = IR \qquad (3)$$

where V is electric potential, R is resistance, and I is the current. Consequently, the voltage distributed with respect to created conductivity (resistivity) distribution. This effect can be clearly observed by comparing voltage distribution of bare antenna case (Fig. 3) with PS I (Fig. S2a) and multilayer PS I (Fig. S2b) cases. In the case of bare antenna, the antenna acts as a capacitor due to absence of conduction between antenna ends, whereas in the presence of PS I, the voltage is distributed over the entire antenna-connector structure as seen in Fig. S2.

Discussion

The PS I due to its extended antenna system with quantum efficiency of 1, has the capability to capture light and efficiently transfer it to excitons [17,26,29]. These excitons coupled with SPP, provide strong means to enhance the electric field of the SPP and allows to modulate the electric field distribution over the whole antenna system. In this work, we have studied four cases in which the PS I acts as the active ingredient in a plasmonic micro antenna. Comparing four different coatings, we see that a single coating and multilayer coatings, enhance the electric field of the antenna concentrating it mostly in the center as can be seen in the experiments (Fig. S2) and in the simulation (Fig. 4b,c) . The enhancement increases with the number of PS I layers. However, when metal colloids are introduced and coupled with the PS I, the field distribution takes a different form. In the case of the Ag and Au PS I colloids, the fields mostly localize at the ends (Fig. 1,2 and SI Fig.3) and standing wave modes are seen in the simulation, most prominent in the Au-PS I case (Fig. 4e). Similar behavior of standing waves formation was observed in the past for light propagation through a free standing micro gold slit coated with up to four layers of PS I[26]. In addition to the field enhancement, coating with PS I allows to modulate the electric field distribution of the antenna by applied voltage, in a non-trivial manner. Comparing to the uncoated antenna, we see that while in uncoated antenna applied voltage created a capacitor, in which only one side of the antenna is amplified by the electric field along the entire antenna length, in the case of coating, the amplification occurs at concentrated locations on the antenna which are determined by the exact coating texture and are

enhanced with increasing voltage. The localization of the electric field over the antenna and its enhancement is attributed to the PS I role, acting as a nano-antenna that captures light efficiently and its extensive ability to generate excitons. To summarize, in this work we demonstrate how a bio-optical active protein that possess highly efficient exciton transfer mechanism, can be integrated in various ways into a micro plasmonic antenna. The integration allows to control electric field distribution of the plasmonic antenna and actively enhance electric field by external application of voltage. This work reports a new physical effect and opens a path to lead variety of novel breaking through applications such as the potential of this hybrid bio-solid state active platform to act as a Bolean logic gate to control optical output signals from plasmonic antenna in optics communications systems.

Methods

Fabrication of the micro antenna on chip. SiO_2/Si sample was spin-coated with double layer electron-beam resist, PMMA 50K A4 at 5000rpm / PMMA 200K A6 @ 5000rpm providing thickness of 100 / 100 nm. Each PMMA layer was subsequently baked for 120 s on a hot plate at 180C. The desired pattern was exposed using a CRESTEC CABLE-9000C high-resolution electron-beam lithography system using 2nAmp, 0.2u-sec for the external pads, and 10pAmp, 0.9u-sec for the plasmonic antenna. Then the samples were developed for 40 s using methyl isobutyl ketone (MIBK) and rinsed with IPA. The samples were subsequently exposed to Ar plasma to etch 10 nm in order to remove leftovers from the pattern, and 2 nm Cr and 18 nm Au, were evaporate using BESTEC thermal evaporator and then immersed in 180 Khz ultrasonic bath with NMP for 3 h for resist liftoff. The fabrication resulted I in an array of 20 antennas 1.5μm in length and ~100nm wide (see Fig.S1). **Unique cysteine mutants** were induced by site-directed mutagenesis in the *psaB* and *psaC* genes of photosystem I (PSI) from *Synechocystis sp*. PCC 6803 resulting in D235C/Y634C (Fig.S5) as earlier described. PSI was isolated from thylakoid membranes by solubilizing with n-dodecyl β-D-maltoside (β-DM) and purification on DEAE-cellulose columns and on a sucrose gradient[24]. The structure of *Synechosystis* sp. PCC 6803 was taken from PDB 6hqb[30].

Adsorption of PSI to the antenna. Adsorption of PS I monolayer was achieved by first cleaning the chip by Ar and O2 (50%:50%) plasma. The chip were then washed in ETOH for 2 minutes, dried and placed in a concentrated solution of PS I for half an hour under illumination and then washed in buffer and deionized water. Multilayers were fabricated by crosslinking of successive PS I layers. This technique insures that the PS I multilayer is covalently bound to the surface in an oriented vectorially fashion.

Surface potential measurements. We used the lift-mode Kelvin probe force microscopy (KPFM) based on dual-line scan imaging, where a lift height of 30 nm was used to avoid interference from the topography. The topography height images were recorded simultaneously with phase and surface potential maps, which were compiled from the amplitude-modulated (AM)-KPFM measurements. All measurements were performed using Dimension Icon AFM system with NanoScope V controller (Bruker) at room temperature in inert atmosphere, when the system is located in the glovebox with oxygen level less of 0.1%.

For KPFM measurements, we used a rectangular, Pt/Ir coated SCM-PIT (Bruker, CA,USA) probe with resonance frequency of 45-100 kHz and spring constant of 4 N/m. To map CPD of the sample, we apply both AC voltage (VAC) and a DC voltage (VDC) to the AFM tip. VAC generates oscillating electrical forces between the AFM tip and sample surface, and VDC nullifies the oscillating electrical forces that originated from CPD between tip and sample surface. The antenna was excited using the white light of the KFM microscope.

The images were captured in the retrace direction with a scan rate of 1.5 Hz. The resolution of the images was 512 samples/line. Nanoscope Analysis Software was used for analysis of the images. Before analysis of the images, the “flatting” and “planefit” functions were applied to each image.

Characterization of film. To verify adsorption of the molecular films the samples were scanned and topography images of the surface were taken. In all cases, the scans indicate good adsorption and the formation of dense layer of molecular film with a thickness ranging from 5 to 15nm. The surface topography of the various coated samples and uncoated reference antenna is shown in Fig. S1b.

A line scan taken across the electrodes (Fig. S1c) shows that the height of the bare uncoated electrode is 26nm±0.6nm. With the organic coatings it amounts to:

30nm±0.8, 34nm±0.9nm, 36nm±1.2 and 41nm±1.8nm for the single PS I layer, Ag-PS I colloids, Au-PS I colloids and PS I multilayer, respectively.

Optical Simulations. The optical simulations were performed using commercial simulation software Ansys Lumerical FDTD. A broadband plane wave source is placed above the structures (+z side) with the injection axis parallel to the surface normal (-$\hat{z}$). Unpolarized incidence results are obtained from the superposition of simulations performed with both x- and y-polarized illumination. PML boundary conditions were applied at $\pm z$ boundaries, and periodic boundary conditions were applied at $\pm$x and $\pm$y boundaries. The structures are placed on the x-y plane on top of a Si substrate that is placed under the structures (-z side). The Si substrate is embedded into PML layer. Near-field field and power monitors were used to obtain the electric field and absorption distributions. For the material models, Johnson-and-Christy's model is used for Au[31], Palik's model used for Si substrate[32], and our previously published data is used for PS I[26].

References

1. Brongersma, M. L. & Shalaev, V. M. The Case for Plasmonics. *Science* **328**, 440–441 (2010).
2. Schnell, M. *et al.* Controlling the near-field oscillations of loaded plasmonic nanoantennas. *Nature Photon* **3**, 287–291 (2009).
3. Curto, A. G. *et al.* Unidirectional Emission of a Quantum Dot Coupled to a Nanoantenna. *Science* **329**, 930–933 (2010).
4. Lal, S., Link, S. & Halas, N. J. Nano-optics from sensing to waveguiding. in *Nanoscience and Technology* 213–220 (Co-Published with Macmillan Publishers Ltd, UK, 2009). doi:10.1142/9789814287005_0022.
5. Kinkhabwala, A. *et al.* Large single-molecule fluorescence enhancements produced by a bowtie nanoantenna. *Nature Photon* **3**, 654–657 (2009).

6. Bozhevolnyi, S. I., Volkov, V. S., Devaux, E., Laluet, J.-Y. & Ebbesen, T. W. Channel plasmon subwavelength waveguide components including interferometers and ring resonators. *Nature* **440**, 508–511 (2006).
7. Krenn, J. R. Watching energy transfer. *Nature Mater* **2**, 210–211 (2003).
8. Dionne, J. A., Sweatlock, L. A., Atwater, H. A. & Polman, A. Plasmon slot waveguides: Towards chip-scale propagation with subwavelength-scale localization. *Phys. Rev. B* **73**, 035407 (2006).
9. Oulton, R. F., Sorger, V. J., Genov, D. A., Pile, D. F. P. & Zhang, X. A hybrid plasmonic waveguide for subwavelength confinement and long-range propagation. *Nature Photon* **2**, 496–500 (2008).
10. Berini, P. & De Leon, I. Surface plasmon–polariton amplifiers and lasers. *Nature Photon* **6**, 16–24 (2012).
11. Yan, H. *et al.* Tunable infrared plasmonic devices using graphene/insulator stacks. *Nature Nanotech* **7**, 330–334 (2012).
12. Zheludev, N. I. A 7-nm light pen makes its mark. *Nature Nanotech* **5**, 10–11 (2010).
13. Maier, S. A. Surface Plasmon Polaritons at Metal / Insulator Interfaces. in *Plasmonics: Fundamentals and Applications* (ed. Maier, S. A.) 21–37 (Springer US, 2007). doi:10.1007/0-387-37825-1_2.
14. RAETHER, H. Surface Plasma Oscillations and Their Applications. *Physics of Thin Films* **9**, 145–261 (1997).
15. Davis, T. J., Gómez, D. E. & Roberts, A. Plasmonic circuits for manipulating optical information. *Nanophotonics* **6**, 543–559 (2017).
16. MacDonald, K. f. & Zheludev, N. i. Active plasmonics: current status. *Laser & Photonics Reviews* **4**, 562–567 (2010).

17. Akhtar, P. *et al.* Two-Dimensional Electronic Spectroscopy of a Minimal Photosystem I Complex Reveals the Rate of Primary Charge Separation. *J. Am. Chem. Soc.* **143**, 14601–14612 (2021).

18. Cohen, M., Shavit, R. & Zalevsky, Z. Observing Optical Plasmons on a Single Nanometer Scale. *Sci Rep* **4**, 4096 (2014).

19. Gerster, D. *et al.* Photocurrent of a single photosynthetic protein. *Nature Nanotech* **7**, 673–676 (2012).

20. Carmeli, I., Frolov, L., Carmeli, C. & Richter, S. Photovoltaic activity of photosystem I-based self-assembled monolayer. **129**, 12352–12353 (2007).

21. Byrdin, M. *et al.* Light Harvesting in Photosystem I: Modeling Based on the 2.5-Å Structure of Photosystem I from Synechococcus elongatus. *Biophysical Journal* **83**, 433–457 (2002).

22. Brettel, K. & Leibl, W. Electron transfer in photosystem I. *Biochimica et Biophysica Acta (BBA) - Bioenergetics* **1507**, 100–114 (2001).

23. Gordiichuk, P. I. *et al.* Solid-State Biophotovoltaic Cells Containing Photosystem I. *Advanced Materials* **26**, 4863–4869 (2014).

24. Frolov, L., Rosenwaks, Y., Carmeli, C. & Carmeli, I. Fabrication of a Photoelectronic Device by Direct Chemical Binding of the Photosynthetic Reaction Center Protein to Metal Surfaces. *Advanced Materials* **17**, 2434–2437 (2005).

25. Carmeli, I. *et al.* A Photosynthetic Reaction Center Covalently Bound to Carbon Nanotubes. *Advanced Materials* **19**, 3901–3905 (2007).

26. Carmeli, I. *et al.* Spatial modulation of light transmission through a single microcavity by coupling of photosynthetic complex excitations to surface plasmons. *Nat Commun* **6**, 7334 (2015).

27. Barhom, H., Carmeli, C. & Carmeli, I. Fabrication of Electronic Junctions between Oriented Multilayers of Photosystem I and the Electrodes of Optoelectronic Solid-State Devices. *J. Phys. Chem. B* **125**, 722–728 (2021).

28. Yao, K. *et al.* Nano-bio hybrids of plasmonic metals/photosynthetic proteins for broad-band light absorption enhancement in organic solar cells. *Journal of Materials Chemistry A* **4**, 13400–13406 (2016).

29. Carmeli, I. *et al.* Broad band enhancement of light absorption in photosystem I by metal nanoparticle antennas. **10**, 2069–2074 (2010).

30. Malavath, T., Caspy, I., Netzer-El, S. Y., Klaiman, D. & Nelson, N. Structure and function of wild-type and subunit-depleted photosystem I in Synechocystis. *Biochimica et Biophysica Acta (BBA) - Bioenergetics* **1859**, 645–654 (2018).

31. Johnson, P. B. & Christy, R. W. Optical Constants of the Noble Metals. *Phys. Rev. B* **6**, 4370–4379 (1972).

32. Edward, D. P. & Palik, I. Handbook of optical constants of solids. (1985).

Supplementary Information

Acknowledgements

K.A. acknowledges support from the Air Force Office of Scientific Research under award number FA9550-17-1-0348.

Affiliations

[1]Faculty of Engineering, Bar-Ilan University Ramat-Gan, 52900 Israel

Zeev Zalevsky, Moshik Cohen, Itai Carmeli

[2] *Department of Electrical and Computer Engineering, Northwestern University, Evanston, Illinois 60208, USA*

Ibrahim Tanriover, Koray Aydin

[3]**department of biochemistry, Tel Aviv University, Tel-Aviv, 69978 Israel**

Chanoch Carmeli, Tirupathi Malavath

[4]**University Center for Nanoscience and Nanotechnology and Department of Materials science and engineering**

Shachar Richter, Itai Carmeli

Institute of nanotechnology and advanced materials, Bar-Ilan University Ramat-Gan, 52900 Israel

Abulafia Yossi, Olga Girshevitz

Contributions

ZZ and MC concived and designed the project, ZZ wrote the paper. IC prefoemed adsorption and synthesis of PS I layers, preformed the experiments and wrote the paper. IT and KY did the simulations and suggested mechanism in the paper. CC designed the PS I mutants and TM grew and purified the PS I for film deposition. AY fabricated the antenna system by photolithography OG helped with KFM measurements and SC corrdinated.

Competing financial interests

The authors declare no competing financial interests.

Corresponding author

Zeev Zalevsky

Supplementary Files

This is a list of supplementary files associated with this preprint. Click to download.

- SI.pdf